

The first gravitational-wave source from the isolated evolution of two 40–100 M_{\odot} stars

Krzysztof Belczynski,¹ Daniel E. Holz,² Tomasz Bulik,¹ Richard O’Shaughnessy,³

¹Astronomical Observatory, Warsaw University, Ujazdowskie 4, 00-478 Warsaw, Poland

²Enrico Fermi Institute, Department of Physics, Department of Astronomy & Astrophysics, and Kavli Institute for Cosmological Physics, University of Chicago, Chicago, IL 60637, USA

³Center for Computational Relativity and Gravitation, Rochester Institute of Technology, Rochester, New York 14623, USA

The merger of two massive $\sim 30 M_{\odot}$ black holes has been detected in gravitational waves (1, *GW150914*). This discovery validates recent predictions (2–4) that massive binary black holes would constitute the first detection. However, previous calculations have not sampled the relevant binary black hole progenitors—massive, low-metallicity binary stars—with sufficient accuracy and input physics to enable robust predictions to better than several orders of magnitude (5–10). Here we report a suite of high-precision numerical simulations of binary black hole formation via the evolution of isolated binary stars, providing a framework to interpret *GW150914* and predict the properties of subsequent binary black hole gravitational-wave events. Our models imply that these events form in an environment where the metallicity is less than 10 per cent of solar; have initial masses of 40–100 M_{\odot} ; and interact through mass transfer and a common envelope phase. Their progenitors likely form either at ~ 2 Gyr, or somewhat less likely, at ~ 11 Gyr after the Big Bang. Most binary black holes form without supernova explosions, and their spins are nearly

unchanged since birth, but do not have to be parallel. The classical field formation of binary black holes proposed in this study, with low natal kicks and restricted common envelope evolution, produces ~ 40 times more binary black holes than dynamical formation channels involving globular clusters (11) and is comparable to the rate from homogeneous evolution channels (12–15). Our calculations predict detections of $\sim 1,000$ black hole mergers per year with total mass of $20\text{--}80 M_{\odot}$ once second generation ground-based gravitational wave observatories reach full sensitivity.

We study the formation of coalescing black hole binaries using the `StarTrack` population synthesis code (16, 17). This method has been updated to account for the formation of massive black hole systems in isolated stellar environments. The new key factors include observationally supported star formation rate, chemical enrichment across cosmic time and revised initial condition for evolution of binary stars. Hitherto, simulations have been unable to achieve the desired predictive power because of the limitations on the input physics (e.g., limited metallicity range) and numerical accuracy. To ensure the dominant contribution from intrinsically rare low-metallicity star-forming environments are adequately sampled, we employ a dense grid of metallicities (32 metallicities) with high precision (20 million binaries each).

Although binary population synthesis is dependent on a number of uncertain physical factors, there has been recent progress in reducing this uncertainty and understanding how it affects predictions. In light of this we consider the following three models to encompass major sources of uncertainty (Methods): M1 represents our “standard” classical formation model for double compact objects composed of two black holes (BH-BH), two neutron stars (NS-NS), or one of each (BH-NS). M2 is our “optimistic” model in which Hertzsprung gap (HG) stars may initiate and survive common envelope (CE) evolution, leading to significantly more binaries being formed. M3 is our “pessimistic” model, where black holes receive high natal kicks, which

disrupts and thereby reduces the number of BH-BH progenitor binaries.

For each generated double compact object merger, with its intrinsic component masses and the redshift of the merger, we estimate the probability that such a merger would have been detectable in the first observing run (O1) of Laser Interferometer Gravitational-Wave Observatory (LIGO) advanced detectors. We adopt a self-consistent model of evolution of stellar populations in Universe (3, 4), and we take the representative noise curve for the O1 run (18), and assume 16 days of coincident science-quality observational time (1).

In Figure 1 we show the formation and evolution of a typical binary system which results in a merger with similar masses and at a similar time to GW150914. Stars that form such mergers are very massive ($40\text{--}100 M_{\odot}$), and at the end of their lives they collapse directly to form BHs (19). Since there is no associated supernova explosion there is also no mass ejection. We allow 10% of the collapsing stellar mass to be emitted in neutrinos. If natal kicks are associated with asymmetric mass ejection (as in our standard model), our prediction is that these massive BHs do not receive natal kicks and their spin directions are the same as that of their progenitor collapsing stars. The binary evolution removes the hydrogen-rich envelope from both binary components, making both stars compact and luminous Wolf-Rayet stars before they collapse to black holes. The first binary interaction is a dynamically stable Roche lobe overflow phase, while the second interaction consists of a common envelope phase that produces a compact binary. After the common envelope phase, the progenitor binary resembles two known high-mass X-ray binaries hosting massive black holes: IC10 X-1 and NGC300 X-1 (20). A massive BH-BH binary (two $\sim 30 M_{\odot}$ BHs) is formed in ~ 5 Myr of evolution, with a relatively wide orbit ($a \sim 50 R_{\odot}$), leading to a long time to coalescence of $t_{\text{merger}} \sim 10$ Gyr. The accretion onto the first BH in the common envelope phase is only modest ($\Delta m \sim 1.5 M_{\odot}$) while accretion from stellar wind of its companion is rather small ($\Delta m < 0.1 M_{\odot}$).

To investigate general aspects of the formation history of GW150914, we select a population

of “GW150914-like” BH-BH mergers with a total redshifted mass of $M_{\text{tot},z} = 54\text{--}73 M_{\odot}$, and then further restrict our sample to binaries that would be detectable in the first observing run (O1) of Laser Interferometer Gravitational-Wave Observatory (LIGO) advanced detectors. The formation channels typical for these massive BH-BH mergers are summarized in Extended Data Table 1.

We find that the most likely progenitor of GW150914 consists of a primary star in the mass range $40\text{--}100 M_{\odot}$ and a secondary in the mass range $40\text{--}80 M_{\odot}$. In our standard model the binary formed in a low metallicity environment ($Z < 10\% Z_{\odot}$; see Extended Data Fig. 1) and in either the early Universe (2 Gyr after the Big Bang) or very recently (11 Gyr after the Big Bang).

The distribution of birth times of these massive BH-BH mergers is bimodal (Fig. 2 and Extended Data Fig. 2), with a majority of systems originating from the distant past (55% of binaries; ~ 2 Gyr after the Big Bang corresponding to $z \sim 3$), and a smaller contribution from relatively young binaries (25%; formed ~ 11 Gyr after the Big Bang corresponding to $z \sim 0.2$). This bimodality arises from two naturally competing effects: On the one hand, most low-metallicity star formation occurs in the early Universe. On the other hand, in contrast to our prior work (3, 4), significantly more low-metallicity star formation is currently expected to occur in the low-redshift Universe (21). Therefore, as is the case with binary neutron stars, we anticipate a significant contribution to the present-day binary black hole merger rate from binary black holes formed in low-redshift low-metallicity star forming regions. The delay time distribution of BH-BH binaries in our simulations follows a $1/t$ distribution. The birth times therefore naturally pile up at low redshifts ($z \sim 0.1\text{--}0.3$) and this gives rise to a low- z peak (Extended Data Fig. 2; a). However, the low-metallicity star formation ($Z < 10\% Z_{\odot}$) responsible for the production of massive BH-BH mergers peaks at redshift ~ 3 (Extended Data Fig. 2; b). The convolution of these two effects produces the bimodal birth time distribution (Extended

Data Fig. 2; c).

These massive “GW150914-like” mergers consist of comparable mass black holes. The vast majority (99.8%) of mergers are found with mass ratios in the range $q = 0.7\text{--}1.0$ (Extended Data Fig. 3), with the mass ratio of GW150914 ($q = 0.82_{-0.21}^{+0.16}$) falling near the center of the expected region. The formation of low mass ratio objects is suppressed because low mass ratio progenitors tend to merge during the first mass transfer event when the more massive component overfills its Roche lobe (22). However, with decreasing total merger mass, the mass ratio extends to lower values. In particular, for the lower mass bin of $M_{\text{tot},z} = 25\text{--}37 M_{\odot}$, mass ratios as low as $q = 0.3$ are also found.

We now use our full sample of double compact object mergers to make predictions for the merger rate density, detection rates, and merger mass distribution. The results are shown in Figure 3 and Extended Data Table 1, where we compare them to the measured values inferred from LIGO O1 observations. We find an overall detection rate consistent with the detection of one significant candidate (GW150914) during the principal 16 day double-coincident period for our “standard” model (M1), while it is inconsistent for our other two models (“optimistic” M2 and “pessimistic” M3; more detail below).

The BH-BH rates inferred from the 16 days of LIGO O1 observations are in the range $2\text{--}400 \text{ Gpc}^{-3} \text{ yr}^{-1}$ (23). For comparison, we estimate the rate density of binary black holes from our population synthesis data set. We consider the full population of binary black holes within a redshift of $z = 0.1$ (i.e., not weighted by their detection probability), and calculate their average source-frame merger rate density. We find a value of $218 \text{ Gpc}^{-3} \text{ yr}^{-1}$ for our standard model (M1), which is in good agreement with the inferred LIGO rate (23). In contrast, our optimistic model (M2) predicts too many mergers, with a rate density of $1,303 \text{ Gpc}^{-3} \text{ yr}^{-1}$, while our pessimistic model (M3) is at the very bottom end of the allowable range with a predicted rate of $6.6 \text{ Gpc}^{-3} \text{ yr}^{-1}$. In our models, the BH-BH merger rate density increases with redshift

(Extended Data Fig. 4). This increase is modest; our predicted source-frame BH-BH merger rate density would double if the cutoff redshift was increased from $z = 0.1$ to $z = 0.6$.

The merger rate density for model with optimistic common envelope (M2) is an order of magnitude larger than the rate estimate from LIGO. This implies that unevolved massive stars (during main sequence and Hertzsprung gap) do not initiate/survive CE (9, 24). In our classical BH-BH formation scheme only evolved stars (during core helium burning) with well-developed convective envelopes are allowed to initiate and survive CE.

Our predictions for the pessimistic model (M3) imply that large natal kicks (with average magnitude $\gtrsim 400 \text{ km s}^{-1}$) are unlikely for massive black holes. This model predicts that an event like GW150914 would happen only 1% of the time, with the detection of any BH-BH system happening less than 10% of the time (Tab. 1). In principle this conclusion applies only to the formation of the first BH in the binary, since high natal kicks lead to disruption of BH-BH progenitors while the binaries are wide. During the formation of the second BH the progenitor binaries are on very close orbits (Fig. 1) and are not disrupted by natal kicks. In Extended Data Figure 4 we show a sequence of models with intermediate BH natal kicks; future observations may allow us to discriminate between these models and constrain the natal kick distribution. If future observations converge on M1 it will indicate no natal kicks nor supernova explosions in massive BH formation (19). A striking ramification of this is the prediction that hot and luminous Wolf-Rayet progenitors of massive BHs (25) should disappear from the sky as a result of direct collapse to a BH. Targeted observational campaigns to search for such phenomena are already underway (26).

Figure 3 shows the relative contribution to the overall merger rate density associated with each bin of total redshifted merger mass $M_{\text{tot},z}$. For comparison, this Figure also shows the fiducial sensitivity ($0.7/VT$) as a function of mass, assuming equal-mass zero-spin binary black holes. This Figure demonstrates that the intersection of the strongly mass-dependent sensitiv-

ity and the intrinsic detectable mass distribution strongly favors sources with total redshifted masses between $25\text{--}73 M_{\odot}$, consistent with our recent work (4), and matching the total redshifted mass of GW150914 ($M_{\text{tot},z} = 70.5 M_{\odot}$). In our simulations the maximum intrinsic mass of a merging BH-BH binary is $M_{\text{tot}} = 140 M_{\odot}$. When accounting for cosmological redshift ($M_{\text{tot},z} = (1 + z)M_{\text{tot}}$), and taking into account the advanced LIGO O1 horizon redshift for this most massive binary ($z = 0.7$), the highest possible observed mass within the O1 run would be $\approx 240 M_{\odot}$.

Spin magnitudes and directions of merging black holes are potentially measurable by LIGO (J). The second-born BH in a BH-BH binary does not accrete mass, and its spin at merger is unchanged from its spin at birth. The first-born BH, on the other hand, has a chance to accrete material from the unevolved companion’s stellar wind or during CE evolution. However, since this is limited either by the very low efficiency of accretion from stellar winds or by inefficient accretion during CE (27, 28), the total accreted mass onto the first-born BH is expected to be rather small ($\sim 1\text{--}2 M_{\odot}$). This is insufficient to significantly increase the spin, and thus the first-born BH spin magnitude at merger is within $\sim 10\%$ of its birth spin.

In our modeling we *assume* that stars that are born in a binary have their spins aligned with the binary angular momentum vector. If massive black holes do not receive natal kicks (e.g., our standard model M1), then our prediction is that BH spins are aligned during the final massive BH-BH merger. We note that our standard model includes natal kicks and mass loss for low-mass BHs ($\lesssim 10 M_{\odot}$), and therefore BH-BH binaries with one or two low-mass BHs may show misalignment. Alternatively, binaries could be born with misalignment and retain it, or misalignment could be caused by the third body, or by interaction of radiative envelope with convective core (29), or misalignment could result from high natal kick on the second-born BH. Several binaries are reported with misaligned spins (30). Therefore, spin alignment of massive merging black holes suggests isolated field evolution, while misaligned spins do not elucidate

formation processes.

As shown in Figure 1, we find that the formation of massive BH-BH mergers is a natural consequence of isolated binary evolution. Our standard model (M1) of BH-BH mergers fully accounts for the observed merger rate density and merger mass (Fig. 3) and mass ratio of two merging BHs (Extended Data Fig. 3) inferred from GW150914.

Our standard formation mechanism (M1) produces significantly more binary black holes than alternative, dynamical channels associated with globular clusters. A recent study (11) suggested globular clusters could produce a typical merger rate of $5 \text{ Gpc}^{-3} \text{ yr}^{-1}$; our standard (M1) model BH-BH merger rate density is ~ 40 times higher: $218 \text{ Gpc}^{-3} \text{ yr}^{-1}$.

However, one non-classical isolated binary evolution channel involving rapidly rotating stars (homogeneous evolution) in very close binaries may also fully account for the formation of GW150914 (12–15). In particular, typical rates of 1.8 detections in 16 days of O1 observations are found (13), which is comparable to our prediction of 2.8. (Tab. 1). Only very massive BH-BH mergers with total intrinsic mass $\gtrsim 50 M_{\odot}$ are formed in this model (12, 13), while we note that our model predicts mergers with mass in a broader range down to $\gtrsim 10 M_{\odot}$. Future LIGO observations of BH-BH mergers may allow us to discriminate between these two very different mass distributions/models.

References and Notes

1. Abbott, B. & et al. Observation of gravitational waves from a binary black hole merger. *Phys. Rev. Lett.* **116**, 061102 (2016).
2. Belczynski, K. *et al.* The effect of metallicity on the detection prospects for gravitational waves. *Astrophys. J. Lett.* **715**, L138–L141 (2010).

3. Dominik, M. *et al.* Double Compact Objects III: Gravitational-wave Detection Rates. *Astrophys. J.* **806**, 263 (2015).
4. Belczynski, K. *et al.* Compact Binary Merger Rates: Comparison with LIGO/Virgo Upper Limits. *Astrophys. J.* **819**, 108 (2016).
5. Tutukov, A. V. & Yungelson, L. R. The merger rate of neutron star and black hole binaries. *Mon. Not. R. Astron. Soc.* **260**, 675–678 (1993).
6. Lipunov, V. M., Postnov, K. A. & Prokhorov, M. E. Black holes and gravitational waves: Possibilities for simultaneous detection using first-generation laser interferometers. *Astronomy Letters* **23**, 492–497 (1997).
7. Nelemans, G., Yungelson, L. R. & Portegies Zwart, S. F. The gravitational wave signal from the Galactic disk population of binaries containing two compact objects. *Astron. Astrophys.* **375**, 890–898 (2001).
8. Voss, R. & Tauris, T. M. Galactic distribution of merging neutron stars and black holes - prospects for short gamma-ray burst progenitors and LIGO/VIRGO. *Mon. Not. R. Astron. Soc.* **342**, 1169–1184 (2003). [astro-ph/0303227](https://arxiv.org/abs/astro-ph/0303227).
9. Belczynski, K., Taam, R. E., Kalogera, V., Rasio, F. A. & Bulik, T. On the Rarity of Double Black Hole Binaries: Consequences for Gravitational Wave Detection. *Astrophys. J.* **662**, 504–511 (2007).
10. Mennekens, N. & Vanbeveren, D. Massive double compact object mergers: gravitational wave sources and r-process element production sites. *Astron. Astrophys.* **564**, A134 (2014).
11. Rodriguez, C. L., Chatterjee, S. & Rasio, F. A. Binary Black Hole Mergers from Globular Clusters: Masses, Merger Rates, and the Impact of Stellar Evolution. *ArXiv e-prints* (2016).

12. Marchant, P., Langer, N., Podsiadlowski, P., Tauris, T. & Moriya, T. A new route towards merging massive black holes. *ArXiv e-prints* (2016).
13. de Mink, S. E. & Mandel, I. The Chemically Homogeneous Evolutionary Channel for Binary Black Hole Mergers: Rates and Properties of Gravitational-Wave Events Detectable by Advanced Ligo. *ArXiv e-prints* (2016).
14. Eldridge, J. J. & Stanway, E. R. BPASS predictions for Binary Black-Hole Mergers. *ArXiv e-prints* (2016).
15. Woosley, S. E. The Progenitor of GW 150914. *ArXiv e-prints* (2016). 1603.00511.
16. Belczynski, K., Kalogera, V. & Bulik, T. A Comprehensive Study of Binary Compact Objects as Gravitational Wave Sources: Evolutionary Channels, Rates, and Physical Properties. *Astrophys. J.* **572**, 407–431 (2002).
17. Belczynski, K. *et al.* Compact Object Modeling with the StarTrack Population Synthesis Code. *ApJS* **174**, 223–260 (2008).
18. <https://dcc.ligo.org/LIGO-G1501223/public>.
19. Fryer, C. L. *et al.* Compact Remnant Mass Function: Dependence on the Explosion Mechanism and Metallicity. *Astrophys. J.* **749**, 91 (2012).
20. Bulik, T., Belczynski, K. & Prestwich, A. IC10 X-1/NGC300 X-1: The Very Immediate Progenitors of BH-BH Binaries. *Astrophys. J.* **730**, 140 (2011).
21. Hirschauer, A. S. *et al.* ALFALFA Discovery of the Most Metal-Poor Gas-Rich Galaxy Known: AGC 198691. *ArXiv e-prints* (2016).

22. Bulik, T., Gondek-Rosinska, D. & Belczynski, K. Expected masses of merging compact object binaries observed in gravitational waves. *Mon. Not. R. Astron. Soc.* **352**, 1372–1380 (2004).
23. Abbott, B. P. *et al.* The Rate of Binary Black Hole Mergers Inferred from Advanced LIGO Observations Surrounding GW150914. *ArXiv e-prints* (2016).
24. Pavlovskii, K. & Ivanova, N. Mass transfer from giant donors. *Mon. Not. R. Astron. Soc.* **449**, 4415–4427 (2015).
25. Eldridge, J. J., Fraser, M., Smartt, S. J., Maund, J. R. & Crockett, R. M. The death of massive stars - II. Observational constraints on the progenitors of Type Ibc supernovae. *Mon. Not. R. Astron. Soc.* **436**, 774–795 (2013).
26. Gerke, J. R., Kochanek, C. S. & Stanek, K. Z. The search for failed supernovae with the Large Binocular Telescope: first candidates. *Mon. Not. R. Astron. Soc.* **450**, 3289–3305 (2015).
27. Ricker, P. M. & Taam, R. E. The Interaction of Stellar Objects within a Common Envelope. *Astrophys. J. Lett.* **672**, L41–L44 (2008).
28. MacLeod, M. & Ramirez-Ruiz, E. Asymmetric Accretion Flows within a Common Envelope. *Astrophys. J.* **803**, 41 (2015).
29. Rogers, T. M., Lin, D. N. C., McElwaine, J. N. & Lau, H. H. B. Internal Gravity Waves in Massive Stars: Angular Momentum Transport. *Astrophys. J.* **772**, 21 (2013).
30. Albrecht, S. *et al.* The BANANA Project. V. Misaligned and Precessing Stellar Rotation Axes in CV Velorum. *Astrophys. J.* **785**, 83 (2014).

Acknowledgments. We are indebted to Grzegorz Wiktorowicz, Wojciech Gladysz and Krzysztof Piszczek for their help with population synthesis calculations, and to Hsin-Yu Chen and Zoheyr Doctor for their help with our LIGO/Virgo rate calculations. We would like to thank thousands of Universe@home users that have provided their personal computers for our simulations. We also want to thank the Hannover GW group for letting us use their ATLAS supercomputer. KB acknowledges support from the NCN grant Sonata Bis 2 (DEC-2012/07/E/ST9/01360). DEH was supported by NSF CAREER grant PHY-1151836. He also acknowledges support from the Kavli Institute for Cosmological Physics at the University of Chicago through NSF grant PHY-1125897 as well as an endowment from the Kavli Foundation. TB acknowledges support from the NCN grant Harmonia 6 (UMO-2014/14/M/ST9/00707). ROS was supported by NSF grant PHY-1505629.

Author Contributions. All authors contributed to the analysis and writing of the paper.

Author Information. Corresponding author email address: chrisbelczynski@gmail.com

Model	Type	O1 rate [yr^{-1}]	O1: 16 days
M1	All	63.18	2.770
	NS-NS	0.052	0.002
	BH-NS	0.231	0.010
	BH-BH	62.90	2.758
	GW150914	11.95	0.524
M2	All	476.1	20.87
	NS-NS	0.191	0.008
	BH-NS	0.796	0.035
	BH-BH	475.1	20.83
	GW150914	110.0	4.823
M3	All	1.985	0.087
	NS-NS	0.039	0.002
	BH-NS	0.014	0.001
	BH-BH	1.932	0.085
	GW150914	0.270	0.012

Table 1: **Expected detection rate and number of detections:** The first column marks: standard (M1), optimistic common envelope (M2), and high BH kicks (M3) models. The third column lists the expected detection rate R_d per unit double-coincident time (both LIGO detectors operating at appropriate sensitivity), for a network comparable to O1, shown for different classes of mergers. The fourth column shows $R_d T$, where $T = 16$ days is the analysis time relevant for the rate estimate for GW150914 (23). Entries marked with “GW150914” are for the subpopulation of BH-BH mergers with total redshifted mass in the range $M_{\text{tot},z} = 54\text{--}73 M_\odot$.

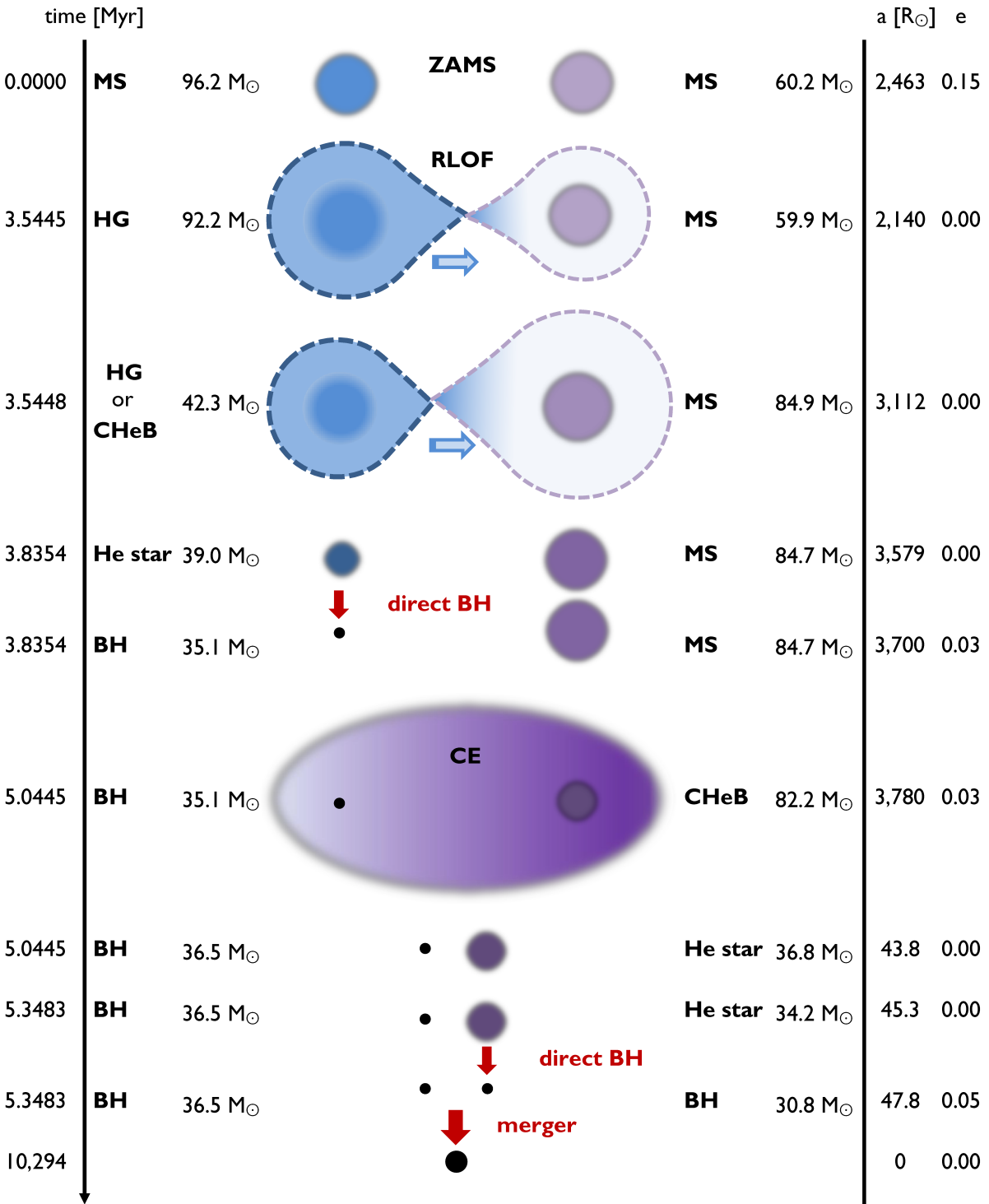


Figure 1: **Example binary evolution leading to a BH-BH merger similar to GW150914.** A massive binary star ($96 + 60 M_{\odot}$) is formed in the distant past (2 billion years after Big Bang; $z \sim 3.2$) and after five million years of evolution forms a BH-BH system ($37 + 31 M_{\odot}$). For the ensuing 10.3 billion years this BH-BH system is subject to angular momentum loss, with the orbital separation steadily decreasing, until the black holes coalesce at redshift $z = 0.09$. This example binary formed in a low metallicity environment ($Z = 3\% Z_{\odot}$).

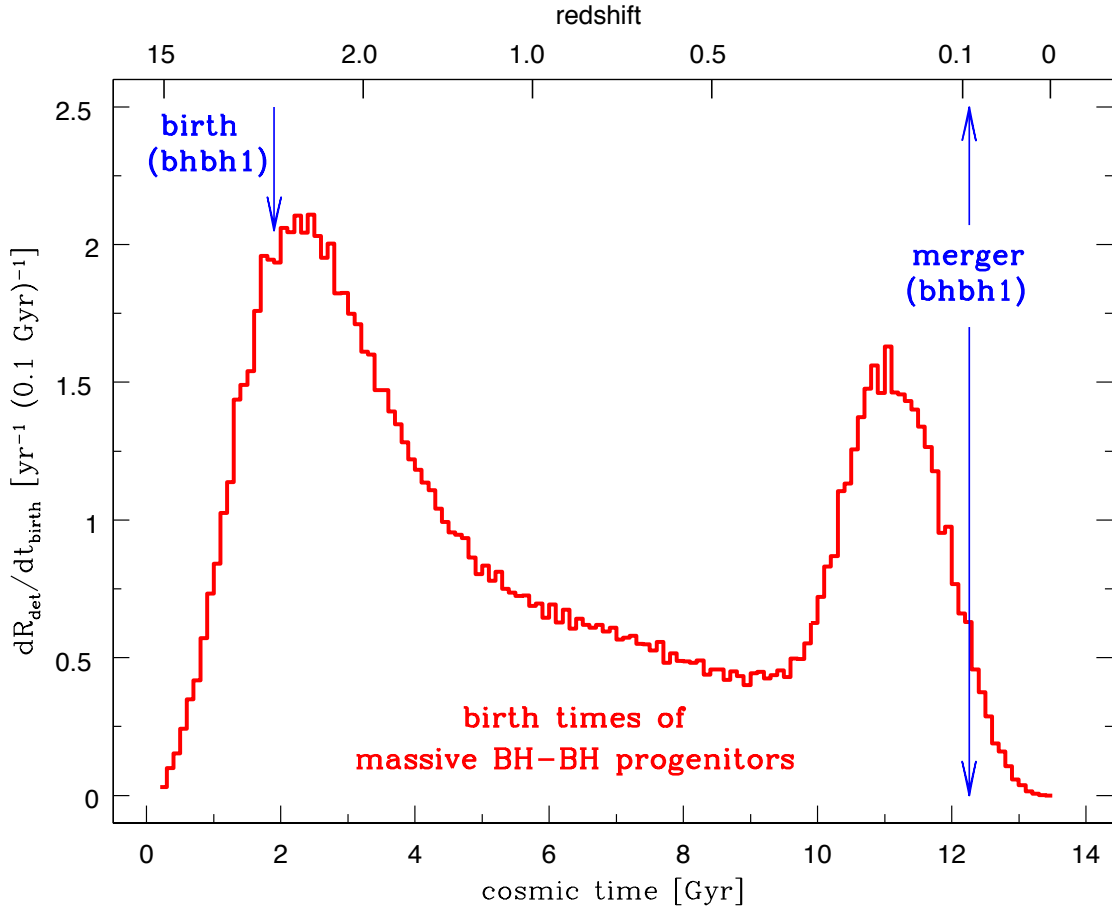


Figure 2: **Birth times of GW150914-like progenitors across cosmic time.** Half of the binaries that form BH-BH mergers detectable in O1 with total redshifted mass in the range $M_{\text{tot},z} = 54\text{--}73 M_{\odot}$ were born within 4.7 Gyr of the Big Bang (corresponding to $z > 1.2$). The birth and merger times of binary from Figure 1 is marked; it follows the most typical evolutionary channel for massive BH-BH mergers (BHBH1 in Extended Data Tab. 1). Note that the merger redshift of GW150914 is $z = 0.088$. The bimodal shape of the distribution originates from a combination of the BH-BH delay time distribution with the low-metallicity star formation history (Extended Data Fig. 2 for details).

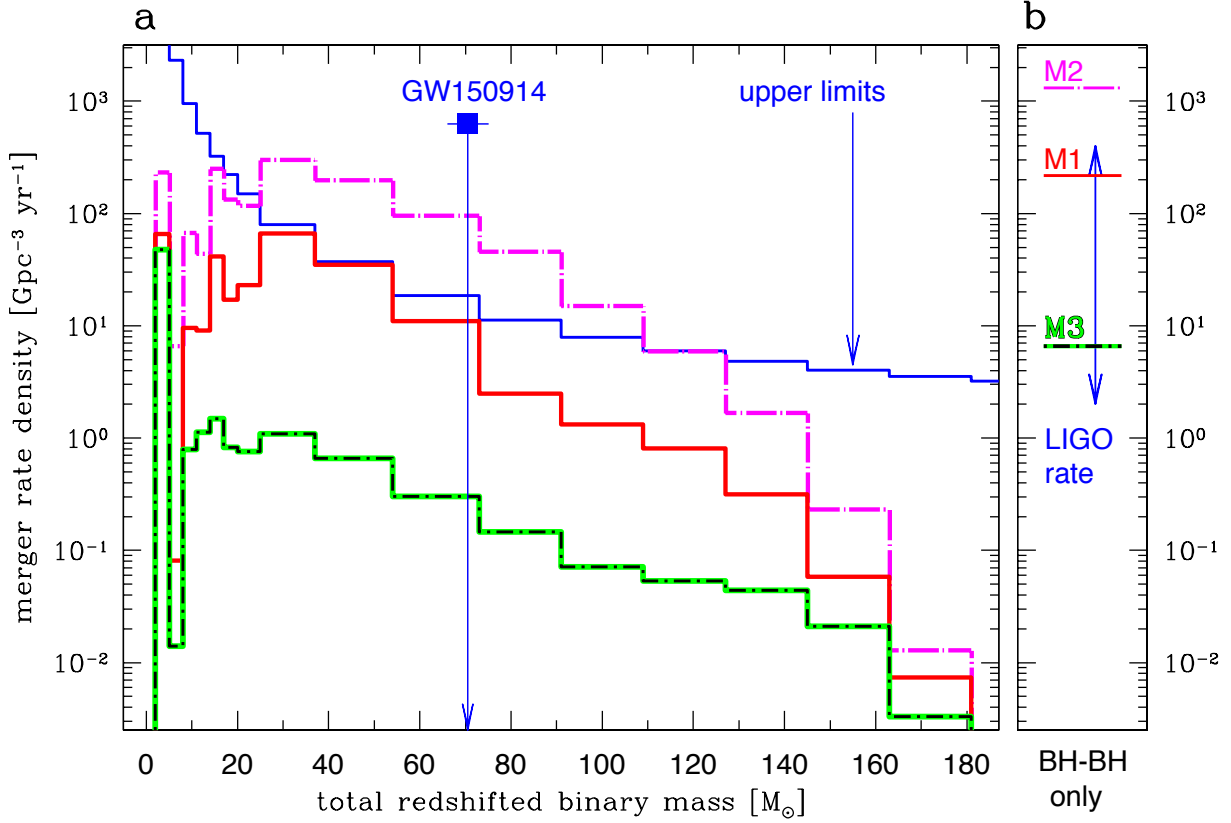


Figure 3: **Comparison of merger rates and masses with LIGO O1 results:** for standard (M1), optimistic CE (M2), and pessimistic high BH kicks (M3) models. **a**, Total redshifted binary merger mass distribution. GW150914 ($70.5 M_{\odot}$: blue square with 90% confidence interval in mass). The blue line shows the fiducial estimate of the sensitivity of the 16 day O1 run. A comparison of the shapes of the blue and red curves suggests that the most likely detections for M1 are BH-BH mergers with mass in the range 25–73 M_{\odot} . NS-NS mergers (first bin) and BH-NS mergers (next five bins) are well below the estimated sensitivity, and thus detections in O1 are not expected. The rate densities are in the detector rest frame. **b**, Comparison of the LIGO BH-BH rate estimate with our models. The LIGO value of 2–400 Gpc $^{-3}$ yr $^{-1}$ (90% credible range) compares well with our standard and high BH natal kick models. The rate densities are in the source rest frame. **Updated version of this figure with the most recent LIGO observations may be found at:** www.syntheticuniverse.org/stvsgwo.html

The Methods

Our Monte Carlo evolutionary modeling is performed with the `StarTrack` binary population synthesis code (16). In particular, we incorporate a calibrated treatment of tidal interactions in close binaries (17), a physical measure of the common envelope (CE) binding energy (31, 32), and a rapid explosion supernova model that reproduces the observed mass gap between neutron stars and black holes (19, 33). Our updated mass spectrum of black holes shows a strong dependence on the metallicity of the progenitor stars (Extended Data Fig. 5). In galaxies with metallicities similar to the Milky Way ($Z = Z_{\odot} = 0.02$) black holes formed out of single massive stars (initial mass $M_{\text{ZAMS}} = 150 M_{\odot}$) reach a maximum mass of $M_{\text{BH}} = 15 M_{\odot}$, while for very low metallicity ($Z = 0.0001 = 0.5\% Z_{\odot}$) the maximum mass becomes $M_{\text{BH}} = 94 M_{\odot}$. The above input physics represents our standard model (M1), which is representative of our classical formation scheme for double compact objects (BH-BH, BH-NS, and NS-NS).

We have adopted specific values for a number of evolutionary parameters. Single stars are evolved with calibrated formulae based on detailed evolutionary calculations (34). Massive star winds are adopted from detailed studies of radiation driven mass loss (35). For the Luminous Blue Variable phase the high mass loss rate is adopted ($1.5 \times 10^{-4} M_{\odot} \text{ yr}^{-1}$). Binary interactions, and in particular the stability of RLOF, is judged based on binary parameters: mass ratio, evolutionary stage of donor, response to mass loss, and behavior of the orbital separation in response to mass transfer. The orbital separation is additionally affected by gravitational radiation, magnetic braking, and angular momentum loss associated

with systemic mass loss. During stable RLOF we assume that half of the mass is accreted onto the companion, while the other half ($1 - f_a = 0.5$) is lost with specific angular momentum ($dJ/dt = j_{\text{loss}}[J_{\text{orb}}/(M_{\text{don}} + M_{\text{acc}})](1 - f_a)dM_{\text{RLOF}}/dt$ with $j_{\text{loss}} = 1.0$ (36)). CE is treated with energy balance with fully effective conversion of orbital energy into envelope ejection ($\alpha = 1.0$), while the envelope binding energy for massive stars is calibrated by a parameter λ that depends on star radius, mass, and metallicity. For massive stars $\lambda \approx 0.1$ is adopted (32). During CE compact objects accrete at 10% Bondi-Hoyle rate as estimated by recent hydrodynamical simulations (27, 28). Our CE is done “instantaneously”, so the time at the beginning and end of CE is exactly the same (see Fig. 1); the time duration of CE has no impact on our results.

We consider two extra variations of the binary evolution input physics. In one model (M2) we test highly uncertain CE physics (37) and we allow for Hertzsprung gap (HG) stars to initiate and survive CE evolution. This is an optimistic assumption, since these stars may not allow for CE evolution (24), nor survive as a binary if CE does happen (9). For comparison, in our standard model we allow only evolved stars with a deep convective envelope (core Helium burning stars) to survive CE.

In the opposite extreme, we employ a model (M3) where black holes receive high natal kicks. In particular, each BH gets a natal kick with its components drawn from a 1-D Maxwellian distribution with $\sigma = 265 \text{ km s}^{-1}$, independent of BH mass. Such high natal kicks are measured for Galactic pulsars (38). This is a pessimistic assumption, as high natal kicks tend to disrupt BH-BH progenitor binaries. This assumption is not yet excluded based on electromagnetic observations (4). In contrast, in our standard model BH natal kicks decrease with BH mass. In particular, for massive BHs that form through direct collapse of an entire star to a BH with no supernova explosion ($M_{\text{BH}} \gtrsim 10 M_{\odot}$ for solar metallicity; $M_{\text{BH}} \gtrsim 15 M_{\odot}$ for $Z = 10\% Z_{\odot}$; and $M_{\text{BH}} \gtrsim 15\text{--}30 M_{\odot}$ for $Z = 1\% Z_{\odot}$) we assume no natal kicks (19). We

have also calculated a series of models with intermediate BH kicks (see Extended Data Fig. 4): $\sigma = 200 \text{ km s}^{-1}$ (model M4), $\sigma = 130 \text{ km s}^{-1}$ (model M5), $\sigma = 70 \text{ km s}^{-1}$ (model M6).

For each evolutionary model we compute 2×10^7 massive binaries for each point on a grid of 32 sub-models covering a wide range of metallicities: $Z = 0.0001, 0.0002, 0.0003, 0.0004, 0.0005, 0.0006, 0.0007, 0.0008, 0.0009, 0.001, 0.0015, 0.002, 0.0025, 0.003, 0.0035, 0.004, 0.0045, 0.005, 0.0055, 0.006, 0.0065, 0.007, 0.0075, 0.008, 0.0085, 0.009, 0.0095, 0.01, 0.015, 0.02, 0.025, 0.03$. We assume that stellar evolution at even lower metallicities proceeds in the same way as the evolution at $Z = 0.5\% Z_{\odot}$. However, we note that stars with very low metal content (e.g., Population III) may evolve differently than metal-rich stars (39).

Each sub-model is computed with initial distributions of orbital periods ($\propto (\log P)^{-0.5}$), eccentricities ($\propto e^{-0.42}$), and mass ratios ($\propto q^0$) appropriate for massive stars (40). We adopt an initial mass function that is close to flat for low mass stars ($\propto M^{-1.3}$ for $0.08 \leq M < 0.5 M_{\odot}$ and $\propto M^{-2.2}$ for $0.5 \leq M < 1.0 M_{\odot}$) and top heavy for massive stars ($\propto M^{-2.3}$ for $1.0 \leq M \leq 150 M_{\odot}$), as guided by recent observations (41). The adopted IMF generates higher BH-BH merger rate densities as compared with the steeper IMF ($\propto M^{-2.7}$ for $1.0 \leq M \leq 150 M_{\odot}$) adopted in our earlier studies (4, 42) as there are more BH-BH merger progenitors in our simulations (43).

A moderate binary fraction ($f_{\text{bi}} = 0.5$) is adopted for stars with mass $M_{\text{ZAMS}} < 10 M_{\odot}$, while we assume that all more massive stars are formed in binaries ($f_{\text{bi}} = 1.0$) as indicated by recent empirical estimates (40, 44).

We adopt an extinction corrected cosmic star formation rate based on numerous multi-wavelength observations (45):

$$\text{SFR}(z) = 0.015 \frac{(1+z)^{2.7}}{1 + [(1+z)/2.9]^{5.6}} M_{\odot} \text{ Mpc}^{-3} \text{ yr}^{-1}. \quad (1)$$

This SFR declines rapidly at high redshifts ($z > 2$). This may be contrasted with some SFR

models that we have used in the past (46) which generated a greater number of stars at high redshifts. This revision will thus reduce the BH-BH merger rate densities at *all* redshifts. Even though the formation of BH-BH binaries takes a very short time (~ 5 Myr), the time to coalescence of two black holes may take a very long time (Fig. 1 and Extended Data Fig. 2).

In our new treatment of chemical enrichment of the Universe we follow the mean metallicity increase with cosmic time (since Big Bang till present). The mean metallicity as a function of redshift is given by

$$\log(Z_{\text{mean}}(z)) = 0.5 + \log\left(\frac{y(1-R)}{\rho_b} \int_z^{20} \frac{97.8 \times 10^{10} \text{ sfr}(z')}{H_0 E(z')(1+z')} dz'\right) \quad (2)$$

with a return fraction $R = 0.27$ (mass fraction of each generation of stars that is put back into the interstellar medium), a net metal yield $y = 0.019$ (mass of new metal created and ejected into the interstellar medium by each generation of stars per unit mass locked in stars), a baryon density $\rho_b = 2.77 \times 10^{11} \Omega_b h_0^2 \text{ M}_\odot \text{ Mpc}^{-3}$ with $\Omega_b = 0.045$ and $h_0 = 0.7$, a star formation rate given by eq. 1, and $E(z) = \sqrt{\Omega_M(1+z)^3 + \Omega_k(1+z)^2 + \Omega_\Lambda}$ with $\Omega_\Lambda = 0.7$, $\Omega_M = 0.3$, $\Omega_k = 0$, and $H_0 = 70.0 \text{ km s}^{-1} \text{ Mpc}^{-1}$. The shape of the mean metallicity dependence on redshift follows recent estimates (45), although the level was increased by 0.5 dex to better fit observational data (47). At each redshift we assume a log-normal distribution of metallicity around the mean, with $\sigma = 0.5$ dex (48). Our prescription (Extended Data Fig. 6) produces more low-metallicity stars than previously (42). Since BH-BH formation is enhanced at low-metallicity (2), our new approach increases the predicted rate densities of BH-BH mergers.

Here we discuss caveats of evolutionary calculations. First, we only consider isolated binary evolution, and thus our approach is applicable to field stars in low density environments. It is possible that dynamical interactions enhance BH-BH merger formation in dense globular clusters (11), offering a completely independent channel.

Second, our predictions are based on a ‘‘classical’’ theory of stellar and binary evolution for

the modeling of massive stars that we have compiled, developed, and calibrated over the last 15 years. We do not consider exotic channels for the formation of BH-BH mergers, such as the one from rapidly rotating stars in contact binaries (49).

Third, our modeling includes only three evolutionary models: a “standard” model consisting of our best estimates for reasonable parameters, as well as “optimistic” and “pessimistic” alternate models. The optimistic model consists of only one change from the standard model: we allow all stars beyond the main sequence to survive the common envelope phase. Alternatively, the pessimistic model also consists of only one change: larger BH natal kicks. We have not investigated other possible deviations from the standard model (e.g., different assumptions of mass and angular momentum loss during stable mass transfer evolution) nor have we checked inter-parameter degeneracies (e.g., models with high BH kicks *and* an optimistic common envelope phase). Albeit with low statistics and limited scope, precursor versions of these computationally demanding studies have already been performed (50); these calculations indicate that our three models are likely to cover the range of interesting effects.

Fourth, our observations are severely statistically limited. We are attempting to draw inferences about our models based on a single detection (GW150914).

It was argued (51) that the formation of GW150914 in isolated binary evolution requires a metallicity lower than 50% Z_{\odot} . This was based on single stellar models (52); stars in close binaries are subject to significant mass loss during RLOF/CE, and they form BHs with lower mass than single stars. Thus in binaries the metallicity threshold for massive BH formation is lower than in single stellar evolution. For example, formation of a *single* 30 M_{\odot} BH requires $Z < 25\% Z_{\odot}$ (Extended Data Fig. 5), while formation of two such BHs in a *binary* requires $Z < 10\% Z_{\odot}$ (Extended Data Fig. 1). The value of this threshold depends on assumptions for the model of stellar evolution, winds, and BH formation processes. The physical models we have adopted yield a threshold of $Z < 10\% Z_{\odot}$, the same as the one obtained with MESA

for homogeneous stellar evolution (12). Our model was calibrated on known masses of BHs, and in particular we do not exceed $15 M_{\odot}$ for Z_{\odot} (the highest mass stellar BH known in our Galaxy). In contrast, single stellar models used to derive the high metallicity threshold produce $25 M_{\odot}$ for Z_{\odot} (52). The highest threshold obtained with binary evolution was reported at the level of $50\% Z_{\odot}$ (14). Such high value of metallicity threshold for the progenitor of GW150914 implies that stars at approximately solar metallicity ($Z = 0.014$) produce BHs as massive as $40 M_{\odot}$ (14). This is neither supported nor excluded by available electromagnetic BH mass measurements (53).

In the following we present calculation of the gravitational radiation signal. The output of `StarTrack` is a binary merger at a given time. We then calculate the gravitational waveform associated with this merger, and determine whether this binary would have been observable by LIGO in the O1 configuration (3, 4).

We model the full inspiral-merger-ringdown waveform of the binaries using the `IMRPhenomD` gravitational waveform template family (54, 55). This is a simple and fast waveform family which neglects the effects of spin (which are not relevant for GW150914). We consider a detection to be given by a threshold $\text{SNR} > 8$ in a single detector, and we use the fiducial O1 noise curve (18). We calculate the face-on, overhead SNR for each binary directly from Eq. 2 of (3). We then calculate the luminosity distance at which this binary would be detected with $\text{SNR} = 8$. Note that as the distance to the binary changes, the observer frame (redshifted) mass also changes, and therefore calculating the horizon redshift requires an iterative process. Once this has been calculated, we then determine the predicted detection rates using Eq. 9 of (3). The effects of the antenna power pattern are incorporated in the p_{det} term in this equation.

Estimate of fiducial aLIGO sensitivity during the 16-day GW150914 analysis is shown in Figure 3. We estimate the sensitivity to coalescing compact binaries using a reference O1 noise curve. We assume that both detectors operate with the fiducial O1 noise curve, which is the same

sensitivity we adopted to calculate compact binary detection rates. For comparison, this model agrees reasonably well with the “early-high” sensitivity model (56). Our expression is a 50th percentile upper limit, assuming no detections. The critical application of this expression is not related to its overall normalization; we are instead interested in its shape, which characterizes the strongly mass-dependent selection biases of LIGO searches.

Using these inputs, our fiducial estimate of the advanced LIGO sensitivity during the first 16 days of O1 for a specific mass bin, ΔM_i , is given by

$$R_{D,\Delta M_i,UL} = \frac{0.7}{V_{\Delta M_i} T}, \quad (3)$$

where T is 16 days, corresponding to the analysis of GW150914 (I), and the volume

$$V_{\Delta M_i} = (\Delta M_i)^{-1} \int dM \int \frac{dz}{1+z} \frac{dV}{dz} p_{\text{det}}(< w, M)$$

is the sensitive volume averaged over the mass bin ΔM_i , and $p_{\text{det}}(< w, M)$ is the orientation-averaged detection probability (3, 4). The function $p_{\text{det}}(< w, M)$ depends on the coalescing binary redshifted mass through the maximum luminosity distance (“horizon distance”) at which a source could produce a response of $\text{SNR} > 8$ in a single detector. To calculate this distance, we adopt the same model for inspiral, merger, and ringdown (54, 55) used in the text to estimate compact binary detection rates. Extended Data Figure 7 shows our estimated horizon redshift as a function of the total redshifted binary merger mass for equal mass mergers.

Code availability. We have opted not to release the population synthesis code `StarTrack` used to generate binary populations for this study.

References and Notes

31. Dominik, M. *et al.* Double compact objects I: The significance of the common envelope on merger rates. *Astrophys. J.* **759**, 52 (2012).

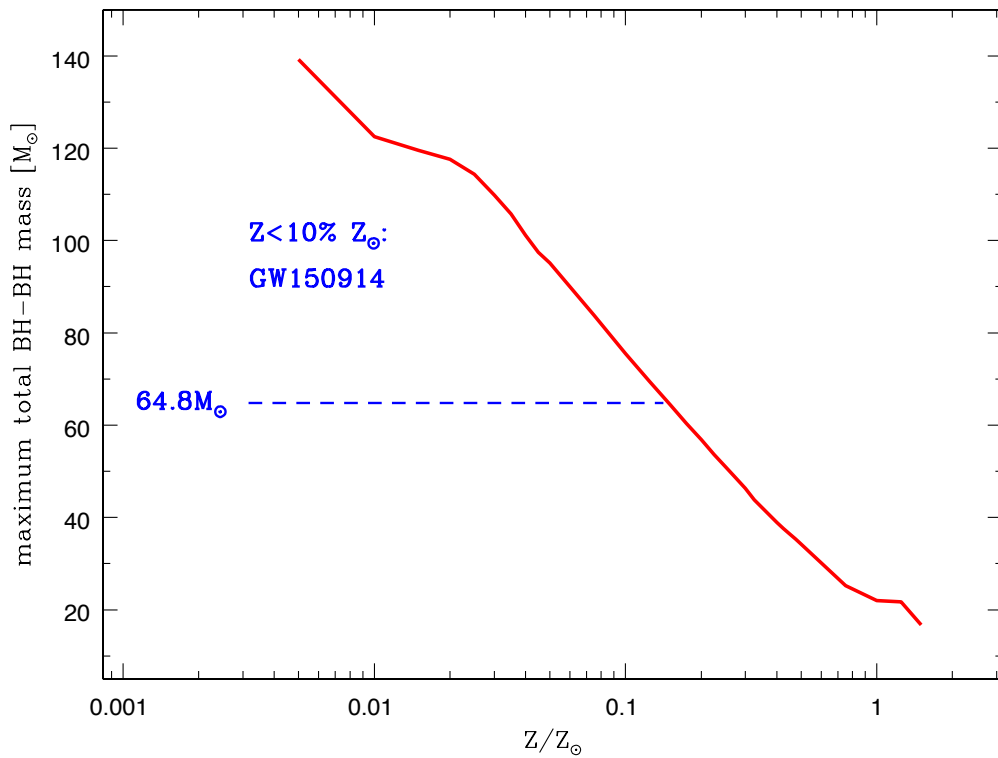
32. Xu, X.-J. & Li, X.-D. ERRATUM: "On the Binding Energy Parameter λ of Common Envelope Evolution". *Astrophys. J.* **722**, 1985–1988 (2010).
33. Belczynski, K., Wiktorowicz, G., Fryer, C. L., Holz, D. E. & Kalogera, V. Missing Black Holes Unveil the Supernova Explosion Mechanism. *Astrophys. J.* **757**, 91 (2012).
34. Hurley, J. R., Pols, O. R. & Tout, C. A. Comprehensive analytic formulae for stellar evolution as a function of mass and metallicity. *Mon. Not. R. Astron. Soc.* **315**, 543–569 (2000).
35. Vink, J. S. The theory of stellar winds. *Ap&SS* **336**, 163–167 (2011).
36. Podsiadlowski, P., Joss, P. C. & Hsu, J. J. L. Presupernova evolution in massive interacting binaries. *Astrophys. J.* **391**, 246–264 (1992).
37. Ivanova, N. *et al.* Common envelope evolution: where we stand and how we can move forward. *A&A Rev.* **21**, 59 (2013).
38. Hobbs, G., Lorimer, D. R., Lyne, A. G. & Kramer, M. A statistical study of 233 pulsar proper motions. *Mon. Not. R. Astron. Soc.* **360**, 974–992 (2005).
39. Szécsi, D. *et al.* Low-metallicity massive single stars with rotation. Evolutionary models applicable to I Zwicky 18. *Astron. Astrophys.* **581**, A15 (2015).
40. Sana, H. *et al.* Binary Interaction Dominates the Evolution of Massive Stars. *Science* **337**, 444 (2012).
41. Bastian, N., Covey, K. R. & Meyer, M. R. A Universal Stellar Initial Mass Function? A Critical Look at Variations. *ARA&A* **48**, 339–389 (2010).

42. Dominik, M. *et al.* Double Compact Objects. II. Cosmological Merger Rates. *Astrophys. J.* **779**, 72 (2013).
43. de Mink, S. E. & Belczynski, K. Merger Rates of Double Neutron Stars and Stellar Origin Black Holes: The Impact of Initial Conditions on Binary Evolution Predictions. *Astrophys. J.* **814**, 58 (2015).
44. Duchêne, G. & Kraus, A. Stellar Multiplicity. *ARA&A* **51**, 269–310 (2013).
45. Madau, P. & Dickinson, M. Cosmic Star-Formation History. *ARA&A* **52**, 415–486 (2014).
46. Strolger, L.-G. *et al.* The Hubble Higher z Supernova Search: Supernovae to $z \sim 1.6$ and Constraints on Type Ia Progenitor Models. *Astrophys. J.* **613**, 200–223 (2004).
47. Vangioni, E. *et al.* The impact of star formation and gamma-ray burst rates at high redshift on cosmic chemical evolution and reionization. *Mon. Not. R. Astron. Soc.* **447**, 2575–2587 (2015).
48. Dvorkin, I., Silk, J., Vangioni, E., Petitjean, P. & Olive, K. A. The origin of dispersion in DLA metallicities. *Mon. Not. R. Astron. Soc.* **452**, L36–L40 (2015).
49. Almeida, L. A. *et al.* Discovery of the Massive Overcontact Binary VFTS352: Evidence for Enhanced Internal Mixing. *Astrophys. J.* **812**, 102 (2015).
50. O’Shaughnessy, R., Kalogera, V. & Belczynski, K. Mapping Population Synthesis Event Rates on Model Parameters. II. Convergence and Accuracy of Multidimensional Fits. *Astrophys. J.* **667**, 1048–1058 (2007).
51. Abbott, B. P. *et al.* Astrophysical Implications of the Binary Black Hole Merger GW150914. *Astrophys. J. Lett.* **818**, L22 (2016).

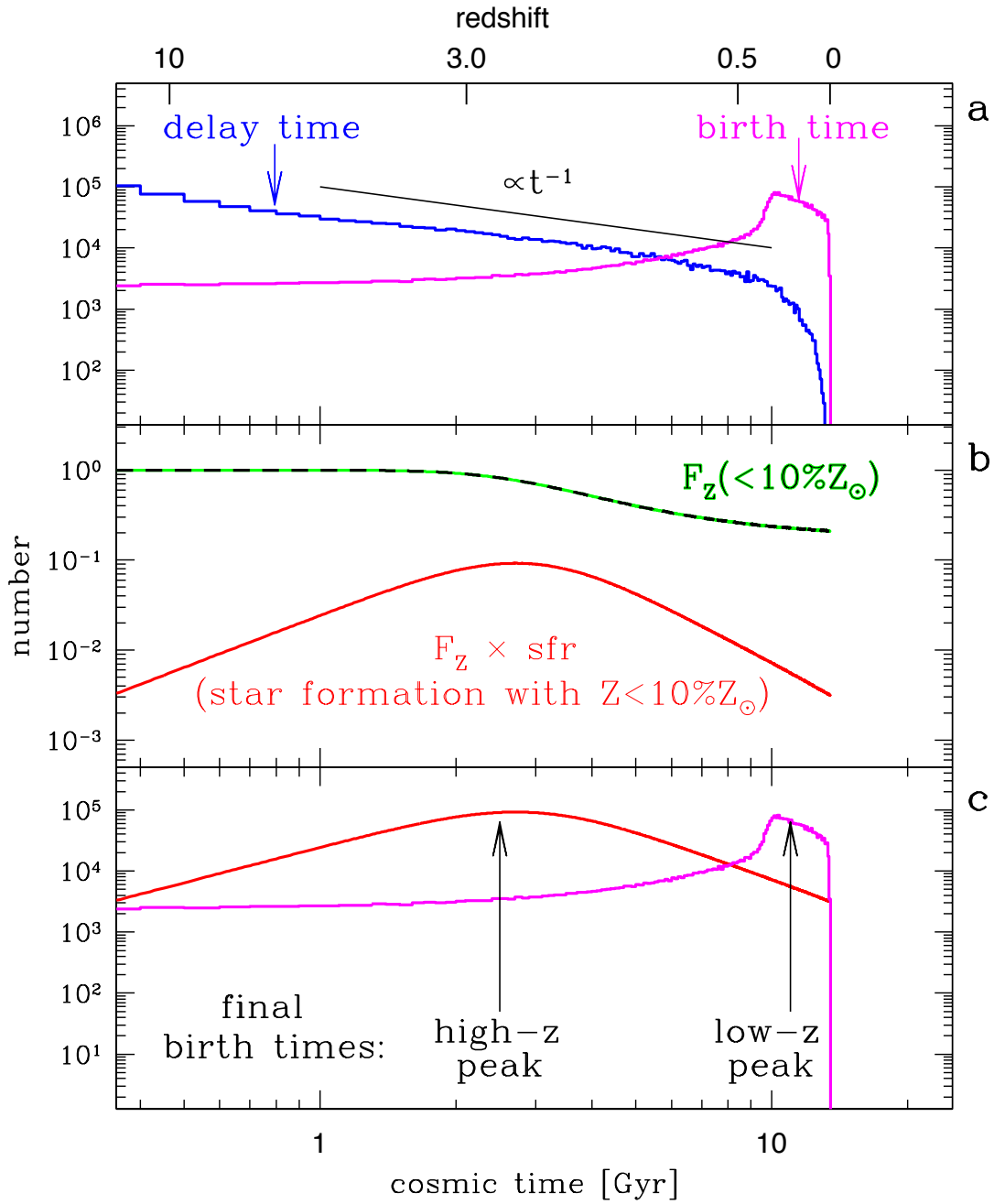
52. Spera, M., Mapelli, M. & Bressan, A. The mass spectrum of compact remnants from the PARSEC stellar evolution tracks. *Mon. Not. R. Astron. Soc.* **451**, 4086–4103 (2015).
53. <https://stellarcollapse.org/bhmasses>.
54. Khan, S. *et al.* Frequency-domain gravitational waves from non-precessing black-hole binaries. II. A phenomenological model for the advanced detector era. *ArXiv e-prints* (2015).
55. Husa, S. *et al.* Frequency-domain gravitational waves from non-precessing black-hole binaries. I. New numerical waveforms and anatomy of the signal. *ArXiv e-prints* (2015).
56. The LIGO Scientific Collaboration *et al.* Prospects for Observing and Localizing Gravitational-Wave Transients with Advanced LIGO and Advanced Virgo. *ArXiv e-prints* (2013).
57. Villante, F. L., Serenelli, A. M., Delahaye, F. & Pinsonneault, M. H. The Chemical Composition of the Sun from Helioseismic and Solar Neutrino Data. *Astrophys. J.* **787**, 13 (2014).

Channel	Evolutionary sequence				all [%]	high- z	mid- z	low- z
BHBH1	MT1(2-1)	BH1	CE2(14-4;14-7)	BH2	79.481	38.045	18.673	22.763
BHBH2	MT1(4-1)	BH1	CE2(14-4;14-7)	BH2	13.461	10.766	1.101	1.594
BHBH3	MT1(4-4)	CE2(4/7-4;7-7)	BH1	BH2	5.363	4.852	0.194	0.317
Other	additional combinations				1.696	0.625	0.421	0.649

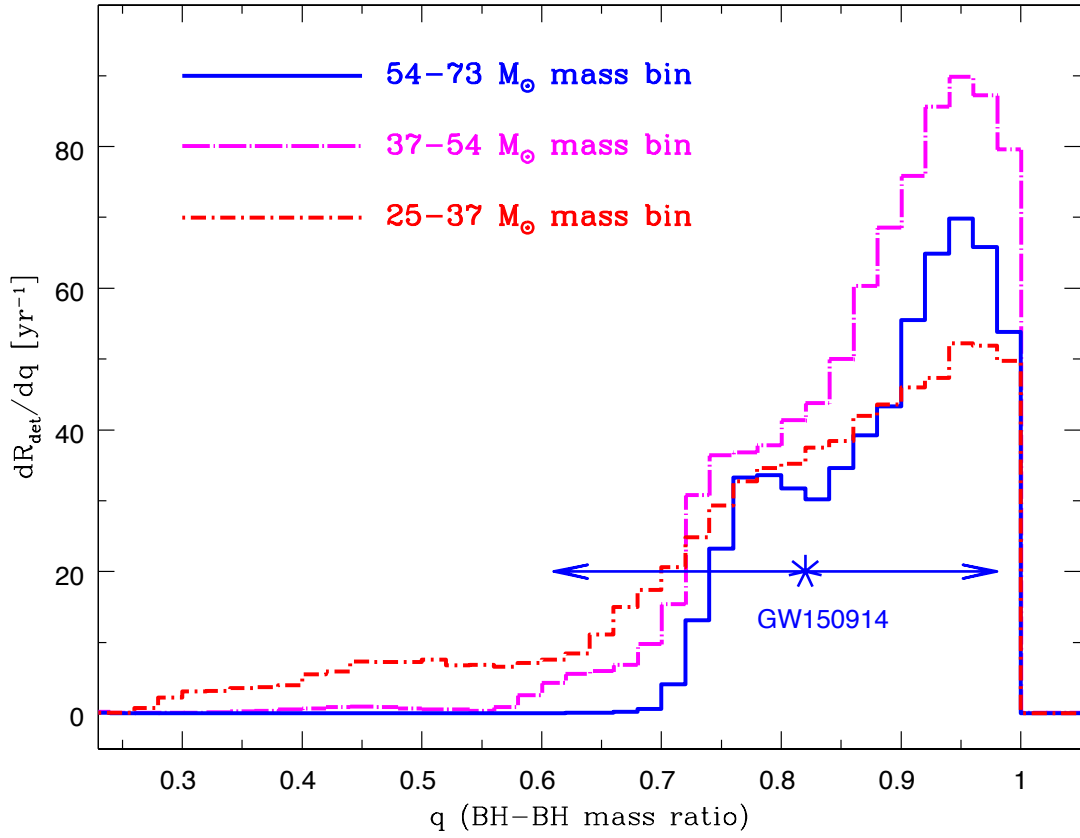
Extended Data Table 1: **Formation channels of massive BH-BH mergers (M1)**: The first two columns identify evolutionary sequences leading to the formation of BH-BH mergers with $M_{\text{tot},z} = 54\text{--}73 M_{\odot}$. The third column lists the formation efficiency. Last three columns list the formation efficiency of BH-BH progenitors born at $z > 1.12$, $1.12 < z < 0.34$, $z < 0.34$. Notation: stable mass transfer (MT), common envelope (CE), BH formation (BH) initiated either by the primary star (1) or the secondary star (2). In parentheses we give the evolutionary stage of stars during MT/(pre;post)CE: main sequence (1), Hertzsprung gap (2), core He-burning (4), helium star (7), BH (14), with the primary star listed first.



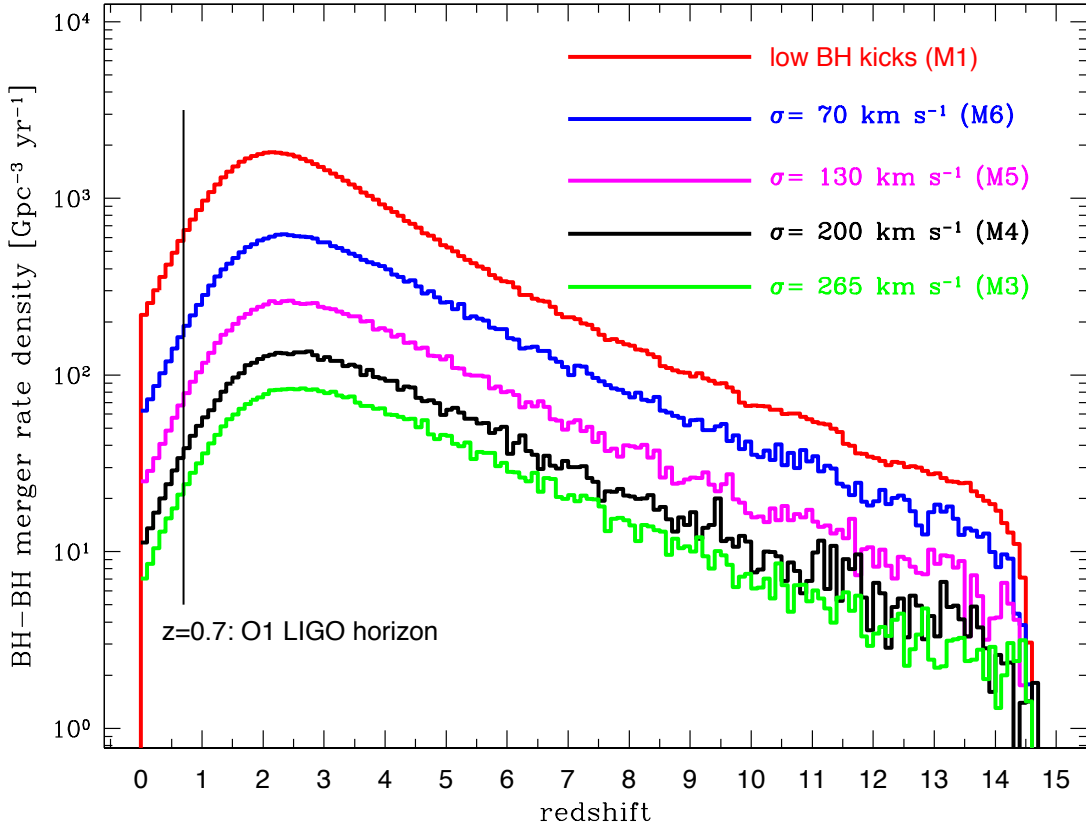
Extended Data Figure 1: **Maximum total mass of BH-BH mergers as a function of metallicity.** Binary stars at metallicities lower than 10% solar can form BH-BH mergers more massive than $M_{\text{tot}} = 64.8 M_{\odot}$. This suggests that GW150914 was formed in a low metallicity environment, assuming it is a product of classical isolated binary evolution. Note that the total *binary* maximum BH-BH mass is not a simple sum of maximum BH masses resulting from *single* stellar evolution; this is a result of mass loss during the RLOF and CE evolution phases in the formation of massive BH-BH mergers (Fig. 1).



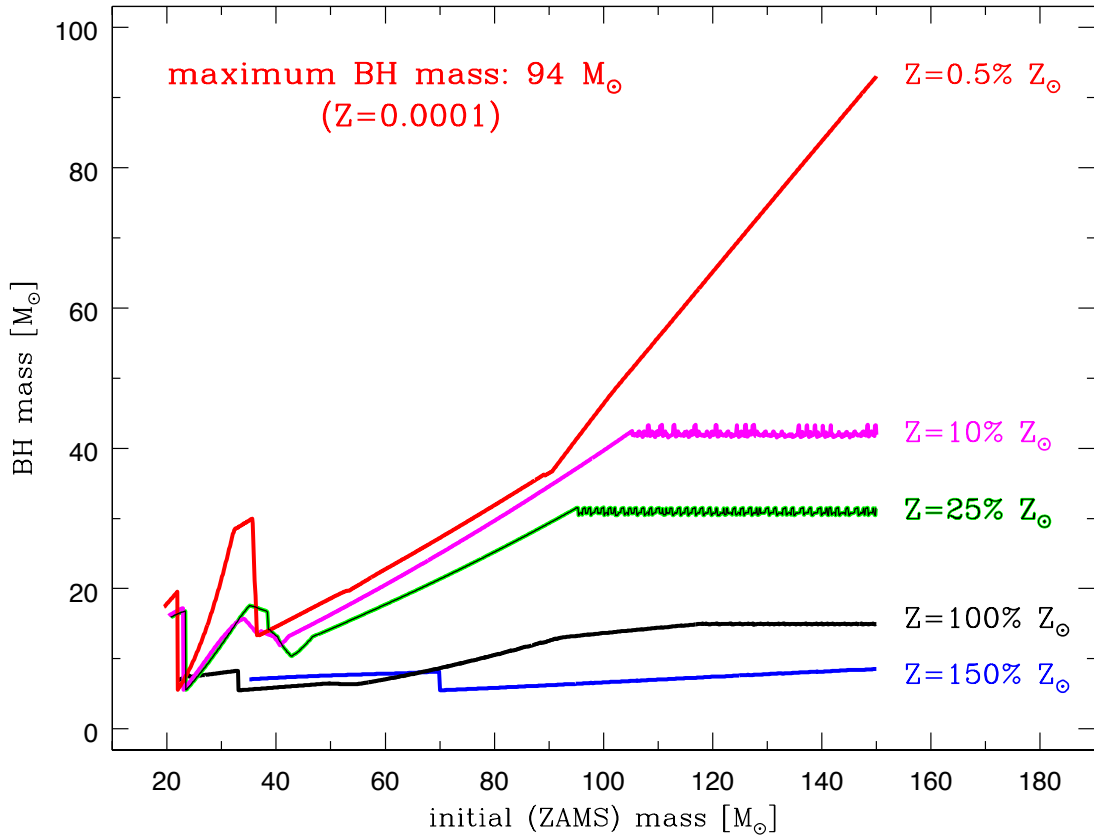
Extended Data Figure 2: **Emergence of bimodal birth time distribution.** **a**, Black hole binaries follow an intrinsic power-law delay time distribution ($\propto t^{-1}$). The birth time ($t_{\text{birth}} = t_{\text{merger}} - t_{\text{delay}}$) is inverted compared to the delay time distribution, with the spread caused by allowing the merger time (t_{merger}) to fall anywhere within the LIGO O1 horizon: $z = 0-0.7$; this generates a peak corresponding to BH-BH progenitors born late with short delay times. **b**, Massive BH-BH binaries are formed only by low-metallicity stars ($Z < 10\% Z_{\odot}$). The fraction of all stars that form at such low- Z (F_Z) decreases with cosmic time making low- Z star formation [$M_{\odot} \text{Mpc}^{-3} \text{yr}^{-1}$] peak at early cosmic time. **c**, Final birth time distribution for massive BH-BH mergers is a convolution of the intrinsic birth times with the low metallicity star formation rate.



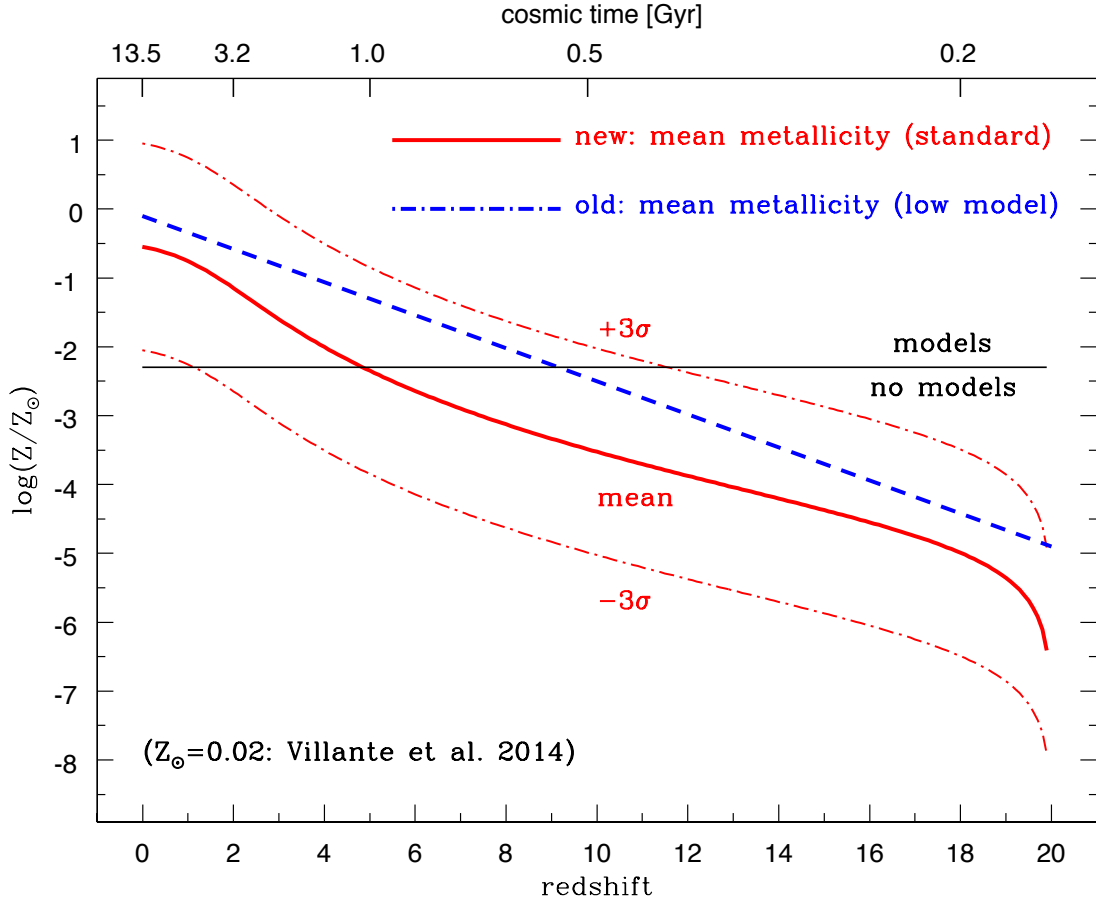
Extended Data Figure 3: **Predicted distribution of BH-BH merger mass ratios.** Standard model (M1) detector frame mass ratio is shown. BH-BH binaries prefer mass ratios of $q \gtrsim 0.7$, with a prominent peak near comparable-mass systems. GW150914 with $q = 0.82^{+0.16}_{-0.21}$ (90% credible range) and with total redshifted mass of $M_{\text{tot},z} = 70.5 M_{\odot}$ falls within the expected region.



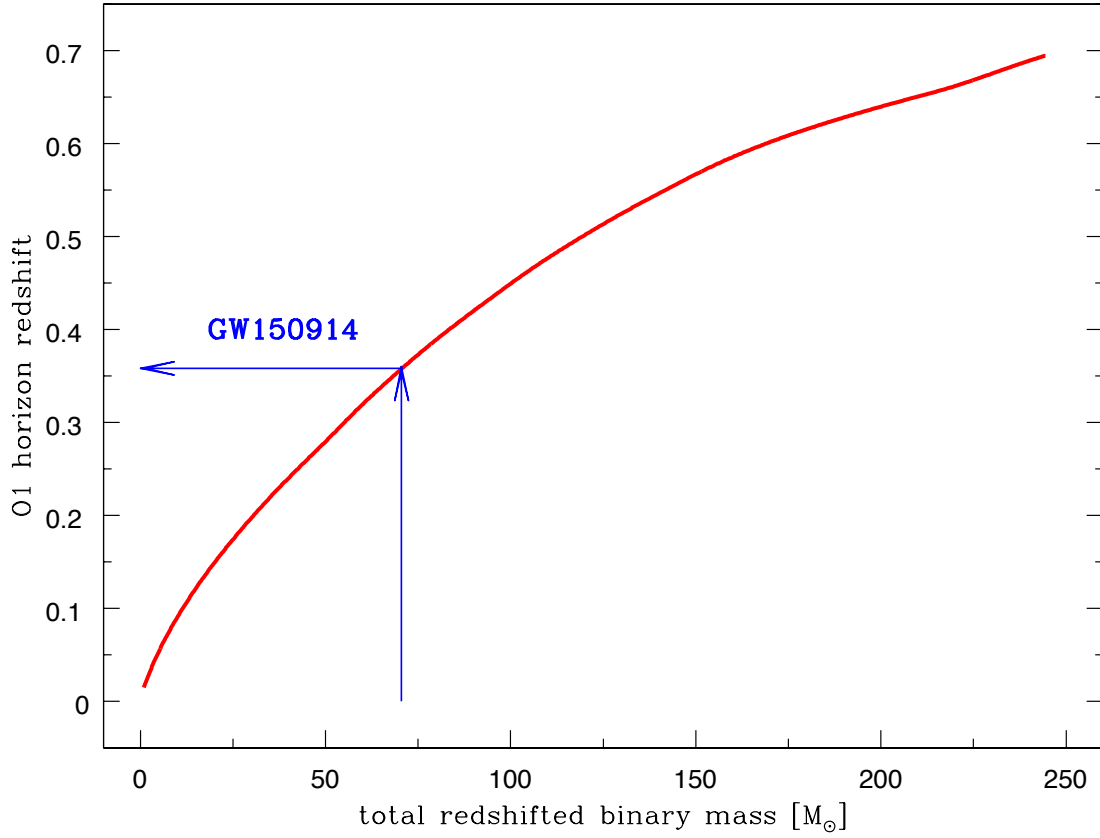
Extended Data Figure 4: **Source frame merger rate density for BH-BH binaries as a function of redshift.** The red line shows the results from our standard model (M1); in this model massive BHs do not get natal kicks. A sequence of models with increasing BH natal kicks (models M6, M5, M4, M3) is shown. The rate density decreases with increasing natal kick. The local merger rate density ($z < 0.1$) changes from $218 \text{ Gpc}^{-3} \text{ yr}^{-1}$ (M1), to $63 \text{ Gpc}^{-3} \text{ yr}^{-1}$ (M6), $25 \text{ Gpc}^{-3} \text{ yr}^{-1}$ (M5), $11 \text{ Gpc}^{-3} \text{ yr}^{-1}$ (M4), $6.6 \text{ Gpc}^{-3} \text{ yr}^{-1}$ (M3). The LIGO estimate ($2\text{--}400 \text{ Gpc}^{-3} \text{ yr}^{-1}$) encompasses all of these models. We mark the O1 LIGO detection horizon ($z = 0.7$; see Extended Data Fig. 7).



Extended Data Figure 5: **BH mass as a function of initial star mass, for a range of metallicities.** These results show calculations for single star evolution with no binary interactions. Our updated models of BH formation show a general increase of BH mass with initial progenitor star mass. There is strong dependence of BH mass on the chemical composition of the progenitor. For example, the maximum BH mass increases from 10–15 M_{\odot} for high metallicity progenitors ($Z = 150\text{--}100\% Z_{\odot}$) to 94 M_{\odot} for low metallicity progenitors ($Z = 0.5\% Z_{\odot}$). Note that the formation of a single 30 M_{\odot} BH requires metallicity of $Z \leq 25\% Z_{\odot}$.



Extended Data Figure 6: **Mean metallicity evolution of the Universe with redshift.** It is assumed that at each redshift the metallicity distribution is log-normal with a standard deviation $\sigma = 0.5\text{dex}$. The blue line denotes the mean metallicity evolution adopted in previous studies. The new relation generates more low metallicity stars at all redshifts. We mark the line above which we can make predictions ($\log(Z/Z_{\odot}) = -2.3$; solar metallicity $Z_{\odot} = 0.02$ (57)) based on actual evolutionary stellar models adopted in our calculations. Below this line we assume that stars produce BH-BH mergers in the same way as in the case of our lowest available model.



Extended Data Figure 7: **Horizon redshift for the first advanced LIGO observational run (O1).** Horizon is given as a function of the total redshifted binary merger mass (assuming equal-mass mergers). For the highest mass mergers found in our simulations ($M_{\text{tot},z} = 240 M_{\odot}$) the horizon redshift is $z_{\text{hor}} = 0.7$. For GW150914 ($M_{\text{tot},z} = 70.5 M_{\odot}$) the horizon redshift is $z_{\text{hor}} = 0.36$.